

Mechanochemical Synthesis of Carbon Nanothread Single Crystals

Xiang Li,^{†,‡} Maria Baldini,[§] Tao Wang,^{‡,||} Bo Chen,^{⊥,○} En-shi Xu,^{‡,||,□} Brian Vermilyea,^{‡,||} Vincent H. Crespi,^{†,‡,||,#} Roald Hoffmann,^{⊥,○} Jamie J. Molaison,[▽] Christopher A. Tulk,[▽] Malcolm Guthrie,[○] Stanislav Sinogeikin,[◆] and John V. Badding^{*†,‡,||,#,○}

[†]Department of Chemistry, Pennsylvania State University, University Park, Pennsylvania 16802, United States

[‡]Materials Research Institute, Pennsylvania State University, University Park, Pennsylvania 16802, United States

[§]Geophysical Laboratory, Carnegie Institution of Washington, Advanced Photon Source, Argonne National Laboratory, Argonne, Illinois 60439, United States

^{||}Department of Physics, Pennsylvania State University, University Park, Pennsylvania 16802, United States

[⊥]Department of Chemistry and Chemical Biology, Baker Laboratory, Cornell University, Ithaca, New York 14853-1301, United States

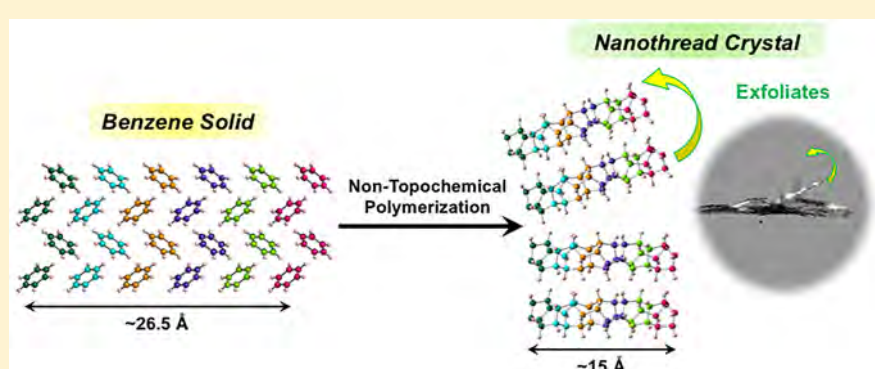
[#]Department of Materials Science and Engineering, Pennsylvania State University, University Park, Pennsylvania 16802, United States

[▽]Neutron Sciences Directorate, Oak Ridge National Laboratory, Oak Ridge, Tennessee 37830, United States

[○]European Spallation Source, ESS ERIC, SE-22100 Lund, Sweden

[◆]High Pressure Collaborative Access Team, Geophysical Laboratory, Carnegie Institution of Washington, Argonne National Laboratory, Argonne, Illinois 60439, United States

Supporting Information



ABSTRACT: Synthesis of well-ordered reduced dimensional carbon solids with extended bonding remains a challenge. For example, few single-crystal organic monomers react under topochemical control to produce single-crystal extended solids. We report a mechanochemical synthesis in which slow compression at room temperature under uniaxial stress can convert polycrystalline or single-crystal benzene monomer into single-crystalline packings of carbon nanothreads, a one-dimensional sp^3 carbon nanomaterial. The long-range order over hundreds of microns of these crystals allows them to readily exfoliate into fibers. The mechanochemical reaction produces macroscopic single crystals despite large dimensional changes caused by the formation of multiple strong, covalent C–C bonds to each monomer and a lack of reactant single-crystal order. Therefore, it appears not to follow a topochemical pathway, but rather one guided by uniaxial stress, to which the nanothreads consistently align. Slow-compression room-temperature synthesis may allow diverse molecular monomers to form single-crystalline packings of polymers, threads, and higher dimensional carbon networks.

INTRODUCTION

Although the profound kinetic stability of carbon covalent bonding yields an extraordinary diversity of well-ordered molecular states, this versatility is not reflected in a similar abundance of well-ordered extended carbon-based solids. Diamond, graphite, certain fullerenes, and some polymers form macroscopic single crystals;^{1–3} carbon nanotubes are well-ordered along their length, but do not form large-scale crystalline packings.⁴ Most other solid-state carbons are either

highly disordered like amorphous or nanoporous carbons or derive from known periodic systems like graphite fluoride and intercalation compounds. Excepting the exquisitely tuned geometries of a limited number of topochemically polymerized systems,^{1,2} the near-equilibrium conditions typically used for production of compact, well-ordered solids tend to defeat the

Received: September 5, 2017

Published: October 17, 2017



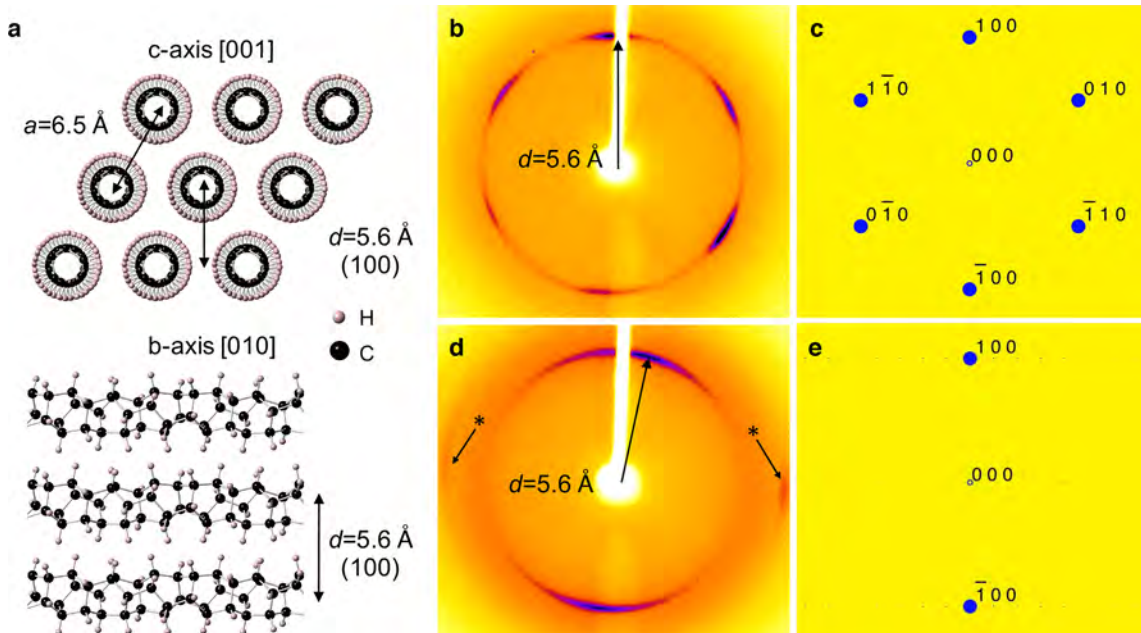


Figure 1. Predicted and observed nanothread crystal diffraction patterns. (a) Polytwistane crystal taken as representative of nanothread packing, viewed down the hexagonal *c*-axis (threads are parallel to it) with a 6.5 Å spacing and (100) planes 5.6 Å apart and a side view down the *b*-axis. (b) X-ray diffraction (300 μm CuK α_1 beam) for a nanothread crystal synthesized from polycrystalline, multiphase benzene shows a hexagonal pattern that matches (c) predicted for the *c*-axis of the polytwistane crystal. (d) Diffraction after 90° rotation of the nanothread crystal, that is, approximately along the *b*-axis, matches the pattern predicted in (e). Diffraction features marked with an asterisk in (d) are from the polymer loop mount.

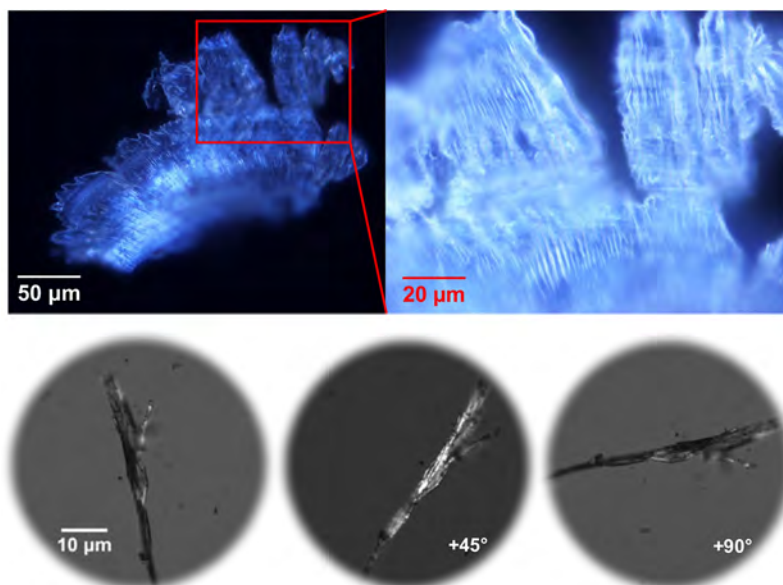


Figure 2. Polarization analysis of nanothread samples from Paris–Edinburgh press. (Top) Mass of nanothreads synthesized from polycrystalline, multiphase benzene between crossed polars. (Bottom) Nanothread fiber between cross polars. After rotation by 45°, transmission increases greatly in the region that is thin and appropriately oriented, demonstrating the presence of strong birefringence. Rotation to 90° re-establishes extinction.

metastable configurational diversity of the carbon–carbon bond that is so evident in organic chemistry. Materials properties across many domains—mechanical, electrical, optical, chemical—often depend critically on the length scale and character of structural order. For example, amorphous silicon as a material is as distinct from the single-crystalline form as single-crystal silicon is from germanium. Macroscopic single crystals can enable advanced applications and an understanding of structure–property relations not possible for polycrystalline or amorphous solid-state carbons.¹ Here we describe a dense, one-

dimensional sp³ carbon-based material with near-single-crystal character over macroscopic length scales.

Benzene exemplifies a large class of multiply unsaturated molecules that can polymerize under pressure or by other means to form multiply connected, extended carbon structures.⁵ Unfortunately, the six new, strong, covalent C–C bonds emanating from each monomer shrink intermolecular separations so dramatically that the products are typically amorphous^{6,7} and bear no simple relation to the reactant benzene phase II molecular crystal.⁸ In contrast, the unit cell of

C_{60} molecules, which are much larger than benzene, shrinks relatively little upon the formation of covalent intermolecular bonds, facilitating a rare topochemical reaction with minimal molecular motion to form a single crystalline extended solid.³ The irreversibility of C–C bond formation between molecules such as benzene provides an additional challenge in realizing crystalline extended solids through non-topochemical routes, one that has been addressed in lower density, porous frameworks by incorporating reversible boroxine bonds.⁹ However, if solid benzene is compressed slowly at room temperature, a one-dimensional sp^3 -bonded product results:¹⁰ These “carbon nanothreads,” depicted in Figures 1a and S1,^{11–14} may combine the highest specific strength known with flexibility, insensitivity to defects, and resilience.^{15,16} However, the nanothread samples reported to date have been polycrystalline, composed of multiple crystallites of different orientations.

Here we report mechanochemical synthesis of macroscopic single crystals of nanothreads with order over much larger dimensions, hundreds of microns, in a consistent, controlled crystallographic orientation. A slower rate of ambient-temperature compression of crystalline benzene monomer than previously employed (see Materials and Methods in the Supporting Information) reproducibly produces single crystals of nanothreads aligned along a near-hexagonal *c* axis, also the axis of uniaxial stress (Figure 1a–e). They exhibit macroscopic striations consistent with one-dimensional character (Figure 2 top) and exfoliate into fibers (Figure 2 bottom). Uniaxial stress thus appears to select a direction of reaction within the three-dimensional benzene phase II crystal, although it is likely that monomer crystallographic orientation and geometrical packing effects also play a role.¹⁷ The tendency of the stress to guide a uniform direction of reaction is so strong that oriented nanothread crystals form not only from appropriately oriented single-crystals of benzene phase II but also from unoriented, polycrystalline mixtures of phases I and II as well and in different types of opposed-anvil pressure apparatus.

RESULTS AND DISCUSSION

We compressed polycrystalline mixtures⁶ of benzene phases I and II (see Figure S2) to 23 GPa in a Paris–Edinburgh press (Figure S3) over 8 h at 2–3 GPa/h from 14 to 19 GPa and 0.6–1.2 GPa/h from 19 to 23 GPa, held them at pressure for 1 h, and released them to ambient pressure over 6–8 h at the same rates in the same pressure ranges as for compression. When in situ measurements were performed, an additional time of 1–2 h was spent at a group of particular fixed pressures, though the above synthesis regime consistently produced nanothread crystals. Diffraction patterns collected after sample recovery to 0.1 MPa with an X-ray beam incident along the prior compression axis reveal 6-fold arcs (Figure 1b) in close agreement with the prediction (Figure 1c) for the *c* axis zone [001] of a representative array of nanothreads with 6.5 Å lattice constant. This confirms the hexagonal unit cell obtained by tentative indexing of a sparse one-dimensional powder diffraction pattern.¹⁰ (For reference, $[uvw]$ indicates a real-space diffraction zone axis, while (hkl) indicates a reciprocal space diffraction plane and $\{hkl\}$ a family thereof.) Multiple crystals produced in separate synthesis runs all show a 6-fold pattern (Figure 1b) under illumination with a 300 μm-diameter laboratory X-ray beam, indicating that crystalline order is macroscopic. The variation in arc intensities in Figure 1b suggests that the crystal tilts slightly off [001]. The form factor for a cylindrical shell of charge as wide as a nanothread drops

off rapidly with increasing scattering angle, thus the intensity of the {100} reflections greatly exceeds that of all others in both simulation and experiment (very weak {200} reflections are observed with a synchrotron X-ray source, Figure S4). Although these data provide compelling evidence for a hexagonal close-packed lattice of cylinders of the same diameter as nanothreads, they cannot discern which of the many enumerated nanothread structures is formed, because the [001] zone does not support $l \neq 0$ reflections.¹⁴ Rotation of the crystal by 90° from the *c*-axis (Figure 1b) reveals 2-fold arcs (Figure 1d) that match the {100} reflections predicted for a beam incident along the [010] axis (Figure 1e), but alas no reflections with $l \neq 0$: The nanothreads are thus likely axially aperiodic (i.e., either helical, short, or disordered along their length, and possibly lacking thread–thread registry); long-range axial periodicity likely awaits further advances in synthetic protocols.

The presence of short 6-fold arcs rather than a uniform diffraction ring shows that the nanothreads also order in the hexagonal *a*–*b* plane (Figure 1b). Polymer fibers oriented solely by stretching/extension or shear typically exhibit fiber diffraction and thus lack this order, and in any case the shear-driven flow in the Paris–Edinburgh press is perpendicular to the thread axis. The 15–20° azimuthal full-width at half-maximum of the 6-fold arcs (Figure 1b) and the width of the 2-fold arcs (Figure 1d) are characteristic of a crystal with a relatively large mosaic spread. We observe single crystals with considerably smaller spreads in diamond cell syntheses, as discussed next.

To gain insight into reaction conditions, synchrotron diffraction data *in situ* in a diamond anvil cell were acquired on polycrystalline mixtures of benzene phases I and II using a 5 × 5 μm beam of 0.4067 Å wavelength (Figures S5 and S6a).⁸ Reaction begins at 16–19 GPa (Figures S7 and S8), that is, we recovered no nanothreads from samples compressed to only 16 GPa. Compression to 23 GPa reproducibly yields 6-fold diffraction patterns which persist upon release of pressure (Figure S6b). These patterns can be indexed to a monoclinic cell with a unique crystallographic *c*-axis (the single cell axis with highest rotational symmetry) angle of 117°, that is, very close to hexagonal. For convenience, we refer to this cell as “pseudohexagonal” and the six narrow arcs as a symmetry-related set {100}. The threads again align closely to the compression axis, which is again parallel to the X-ray beam. These arcs (8–12° fwhm) are narrower in azimuth than those of the Paris–Edinburgh samples (compare Figure S6b to Figure 1b), indicating a smaller mosaic spread in the *a*–*b* plane across the sampling volume of the 5 × 5 μm X-ray beam. They also have narrower 2θ diffraction line widths (Figure S9). The improved order may be due to larger uniaxial stress in the diamond anvil cell.

Modeling suggests that nanothreads are much stiffer than polymers,¹⁸ with persistence lengths of ~100 nm.¹⁵ Consistent with an ordered packing of aligned, stiff threads bound by van der Waals forces (and unlike conventional hydrocarbon polymers or polycrystalline materials), nanothread crystals can be mechanically exfoliated into fibers (Figure 2 bottom) just as graphite can be exfoliated ultimately to graphene. Exfoliated fibers are birefringent, consistent with the optical anisotropy expected from such a structure. Exfoliation into single threads may provide nanoscale building blocks with tunable strength and ductility that can be reassembled and/or functionalized to control properties and processability.¹⁶

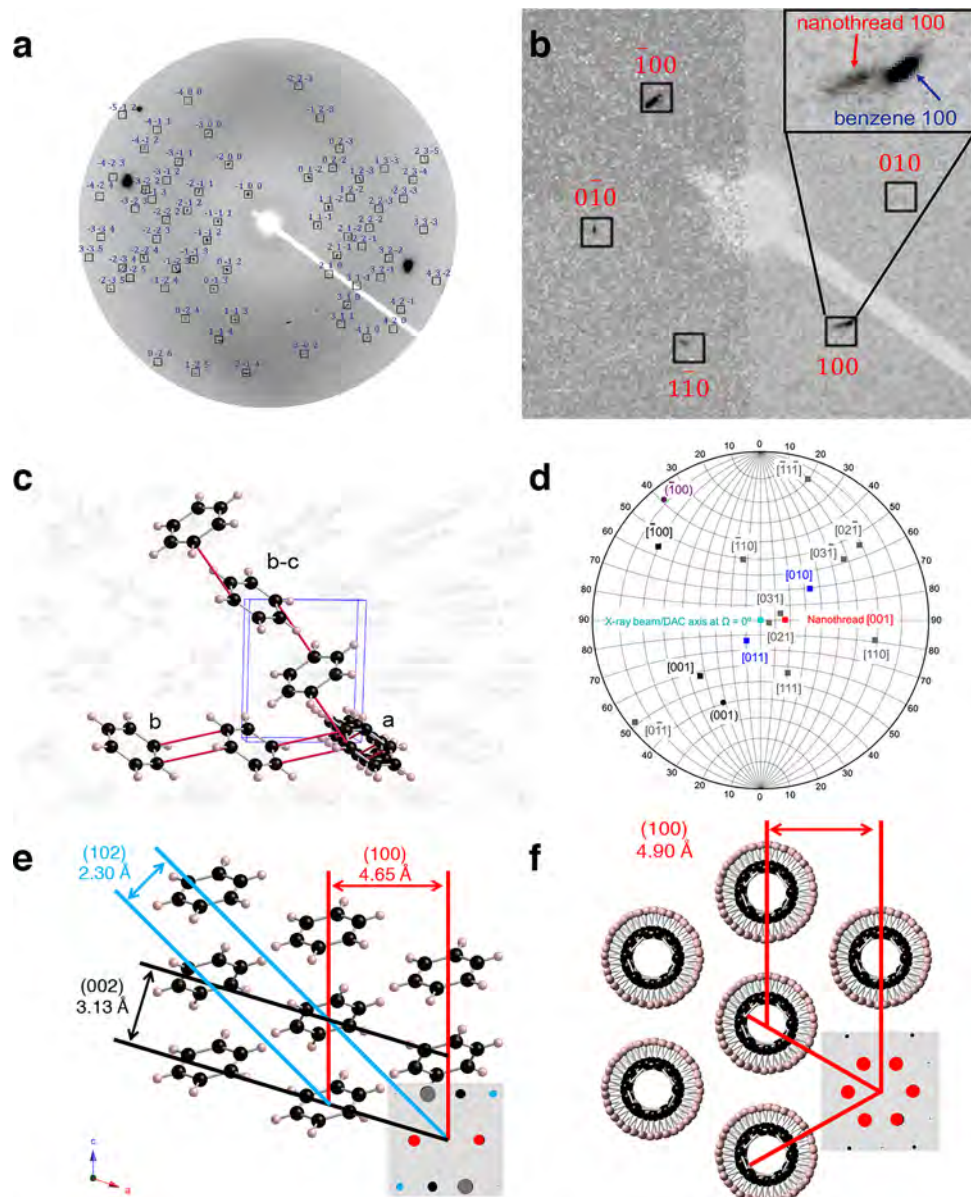


Figure 3. In situ nanothread diffraction at high pressure and deduced spatial relationships. (a) Indexed diffraction pattern collected upon increasing pressure to 3.3 GPa for a phase II single crystal. Large dark spots are diamond anvil reflections. (b) Expanded view of diffraction pattern upon increasing pressure to 23 GPa for phase II single crystal showing pseudohexagonal carbon nanothread {100} peaks beginning to appear. The inset shows the benzene (100) peak neighboring the nanothread (100) peak; (010) is >30 counts above background, though difficult to see in the figure. (c) *a*, *b*, and *b-c* columns of benzene molecules along which reaction to form nanothreads is considered; unit cell in blue. (d) Stereographic projection of benzene phase II diffraction planes (*hkl*) and zone axes [*uvw*], showing the angular relationship at 23 GPa of the nanothread crystal [001] *c*-axis to the benzene crystal [100] *a*, [010] *b*, and [011] *b-c* axes. Only the directions and planes on the “north” side of the projection are shown (e.g., [100] is on the south side, 180° from [100]). (e) The monoclinic benzene crystal viewed down the unique *b*-axis, showing diffraction planes and their interplanar spacings at 23 GPa with the orientation and spacing of diffraction spots in the inset. Diffraction planes for the gray spots are not shown. (f) A monoclinic (pseudohexagonal, $\gamma = 117^\circ$) nanothread crystal viewed down the *c* axis with interplanar spacings at 23 GPa. Diffraction planes have the same scale as (d). Note the slight expansion required for the benzene (100) planes to form nanothread (100) planes and the larger shifts required for planes at angles to (100).

It is remarkable that macroscopic aligned single crystals of nanothreads (Figures 1b and S6b) emerge from polycrystalline mixtures of benzene phases I and II compressed in both Paris–Edinburgh and diamond cells in which each grain has a complex three-dimensional crystal structure (Figures S3, S5, and S6a; the diamond cell diffraction patterns confirm that multiple phase I and II crystallites are in the X-ray beam before reaction; similarly, neutron powder diffraction from two phase benzene samples compressed in Paris–Edinburgh cells that

indicate they are polycrystalline (Figure S2)). The reverse of this process, that is, single crystals breaking up into polycrystals due to reaction-induced stresses, is much more common.⁷ Benzene phase II hosts three crystallographically distinct nearest-neighbor stacks of molecules (reaction occurs in phase II, see below). One or more of these stacks may have a geometry that allows collapse into threads by a radical or cycloaddition mechanism.¹³ In appropriately aligned crystallites, uniaxial stress will preferentially bring the molecules in

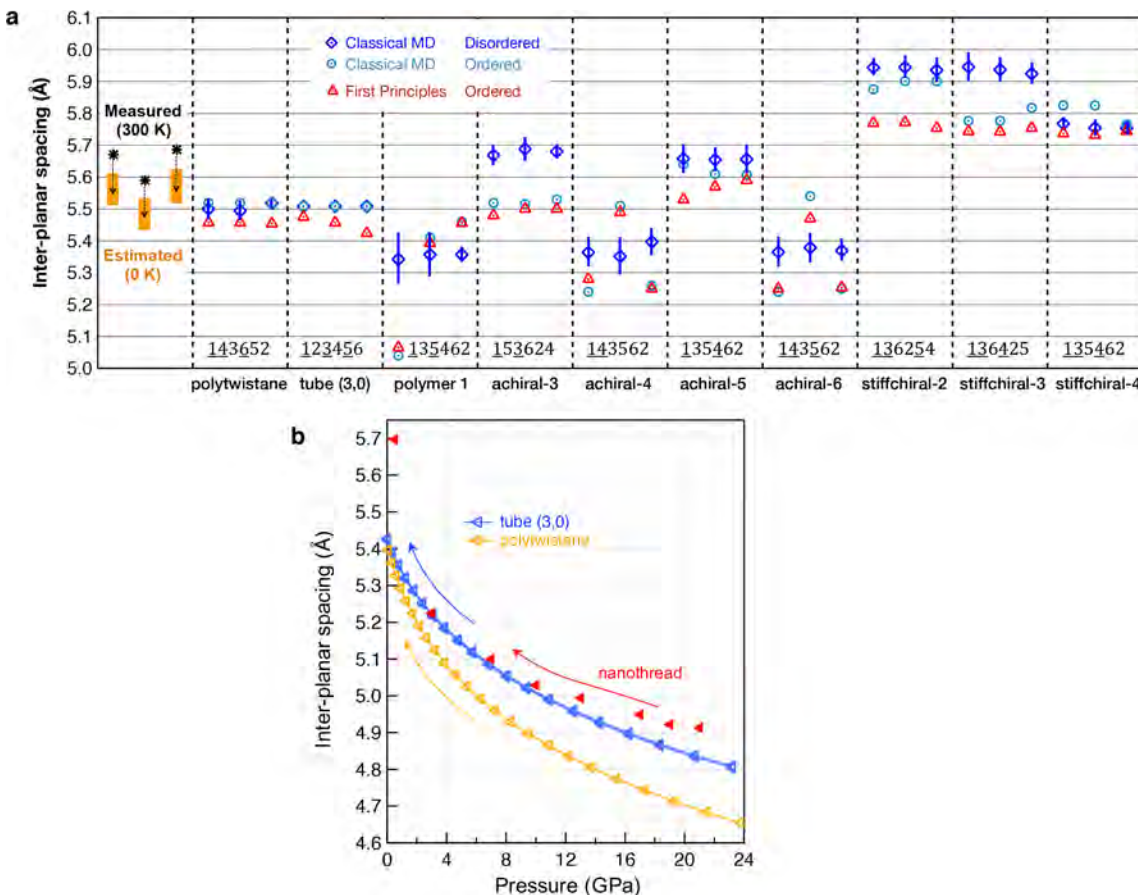


Figure 4. Constraining nanothread structure with experimental and calculated {100} interplanar spacings. (a) Interplanar spacings calculated for candidate achiral and chiral nanothread structures at $T = 0$ (see Figure S1), including both ordered and disordered axial/azimuthal arrangements at empirical and first-principles levels, to show which ones are consistent with the measured interplanar spacings in the nanothreads synthesized from mixed phase I/II benzene. The anticipated shifts in the experimental data due to thermal contraction to $T = 0$ are depicted by orange bars, and the full-width-at-half-maximum over 10 instances of calculated disorder is marked by vertical blue bars. Experimental nanothread {100} interplanar spacings at ambient pressure are from sample synthesized in a diamond cell from polycrystalline, multiphase benzene. (b) Nanothread (100) interplanar spacings during decompression. The threads again formed from a polycrystalline mixture of phases I and II in a diamond cell. Calculated first-principles {100} interplanar spacings derived from lattice parameters are also shown for two representative nanothread crystals.

these stacks closer together (Figure S3). Once initiated, reaction would most easily propagate along the uniaxial stress axis, aided by packing constraints similar to those that operate in nematic liquid crystals. The benzene stacks must contract dramatically along the thread axis (by 40–50%) as nanothreads form, indicating that the reaction cannot be topochemical and further underlining the remarkable fact that well-ordered one-dimensional crystals can be obtained from an uncatalyzed room-temperature reaction involving carbon–carbon bonds. Any crystallites not oriented to react would simply melt upon pressure release; we observe benzene liquid coexisting with the solid nanothreads upon recovery before it evaporates. Remarkably, the order observed in the a – b plane (Figure 1b) appears to propagate through the multiple crystallites selected for reaction. Single-crystal PbS nanosheets have been synthesized by uniaxial stress applied to unaligned packings of nanoparticles, suggesting similar guiding roles for uniaxial stress in the two cases.¹⁹ Speaking more speculatively, the strong kinetic preference for the single lowest-barrier pathway that is implied by our slow compression at low (i.e., room) temperature may also, ironically, facilitate formation of well-ordered nanothread crystals by suppressing less favorable reactions that, for example, cross-link the nascent threads.

To further probe the importance of crystal alignment in nanothread formation, we produced crystals of pure phase II benzene inside a diamond anvil cell by annealing and analyzed the resulting system *in situ* under pressure by the rotating crystal method.^{8,20} Step rotation and continuous wide-angle rotation two-dimensional synchrotron X-ray diffraction patterns were collected on crystals that were larger than the $5 \times 5 \mu\text{m}$ beam between -15° and 15° of ω rotation angle about a vertical axis perpendicular to the horizontal synchrotron beam (the range being limited by the diamond cell geometry).²⁰ At 3.3 GPa, we observed a phase II single crystal (Figure 3a). Upon compression to 23 GPa, five new diffraction spots characteristic of a nanothread crystal were observed at $\omega = 15^\circ$, reasonably close to the axis of compression (Figure 3b); we index these spots with a pseudohexagonal cell and a unique c -axis angle of 117° .²¹ These results show that nanothread synthesis does not require phase I, which in any case lacks suitable benzene contacts (Figures S5 and S10). The “slipped” molecular stacks along the a , b , and b – c axes of benzene phase II (shown in Figure 3c) are instead the most likely candidates for intrastack reaction.¹³ To assess the spatial relationships between the benzene phase II and nanothread crystals, we determined their orientation matrices at 23 GPa.²⁰ The

nanothread crystal that forms has its pseudohexagonal *c* axis oriented 15° from the axis of compression and close to midway between the *b* and *bc* stacks of the phase II crystal (about 27° from either), as shown in Figure 3d. Reaction along the *a* axis can thus be ruled out, since it is nearly orthogonal to the nanothread *c* axis, while the *b* and *b*–*c* stacks of benzene phase II remain viable candidates for nanothread formation.¹³ In accord with this conclusion, we observe no nanothread diffraction peaks for a different phase II single-crystal sample compressed to 23 GPa that had its *c* axis, which has no stacks suitable for reaction,¹³ parallel to the axis of compression and the X-ray beam (see Supporting Information).

As the nanothreads emerge by reaction along a suitable benzene column, a plausible origin of the increase in symmetry from monoclinic benzene to the pseudohexagonal nanothread crystal is the close-packing of extended objects with near-cylindrical symmetry in two dimensions. The candidate *b*-axis benzene stacks must undergo a large rearrangement to form hexagonally packed nanothreads, for example, the cross-section perpendicular to *b* must expand by ~45% along its short axis to match hexagonal packing, as shown in Figure 3e,f. The spacing of the candidate *b*–*c* stacks must change greatly as well (Figure S11) as must any other (less likely) reaction stack. Such large geometric changes are not typical of topochemical reactions.²²

Upon lowering the pressure on the single-crystal sample, the sixth remaining nanothread reflection appears (it was likely not within the range of available ω angles at 23 GPa), and all the reflection intensities increase considerably (Figure S12a,b and S13). As the pressure drops, either further reaction to form more threads occurs or the nanothreads that have already formed optimize their hexagonal packing, or both. These diffraction arcs are quite narrow (Figure S12a,b).

Although the existing diffraction data cannot uniquely determine the atomic-scale structure along the thread axis, the high level of precision in the observed pseudohexagonal lattice parameters can be combined with careful first-principles density functional theory, and empirical molecular dynamics to significantly constrain which of the candidate nanothread bond topologies (Figure S14) are consistent with the experimental packing.²³ As shown in Figure 4a, simulations reveal that many of these candidates are not consistent with the experimental {100} interplanar spacings, in this case those measured at 0.1 MPa for the sample that was synthesized from polycrystalline benzene (when shrunk by 1–3% to account for thermal contraction to the *T* = 0 calculations).^{24,25} Of those thread structures that are consistent with the experimental lattice parameters, polytwistane (143652) and tube (3,0) (123456) both have a single symmetry-distinct carbon site, although on-thread structural disorder could increase this number; others such as rotationally ordered achiral-3 or achiral-5 have multiple such sites, and expansion of the analysis to include degree 4 threads could yield additional options. Several other thread structures examined are too loosely packed along at least one dimension.

Based on the optimized packing geometries, we calculated the lattice parameters of tube (3,0) and polytwistane within density functional theory from 0 to 24 GPa and then back to zero, with one thread per near-hexagonal unit cell (Figure 4b). The compressibilities of both candidate threads match reasonably well to the experimental decompression curves, keeping in mind that the experimental data includes an estimated 1–3% thermal expansion from 0 to 300 K. Modest on-thread structural disorder that does not substantially change

the local diameter of the thread is unlikely to significantly degrade this agreement. One possible discrepancy is a steeper upslope of the experimental curves below 3 GPa, suggesting that slight imperfections in the experimental nanothread packing may be squeezed out by moderate pressure; taking this into account then favors the more densely packed options in Figure 4a. The weaker nature of this discrepancy in the single-phase sample of Figure S15 is consistent with this scenario.

CONCLUSIONS

The robust, reproducible formation of nanothread crystals from benzene suggests that other unsaturated molecular crystals that are unsuitable for topochemical reaction may nevertheless form single-crystalline packings of polymers or nanothreads upon slow uniaxial compression. For example, we have recently synthesized single crystals of carbon/nitrogen nanothreads from pyridine, which has a different crystal structure from benzene (X. Li, unpublished results). Slow, cold compression may thus provide a general route to synthesizing single-crystalline packings of low-dimensional fully or partially saturated carbon-based nanomaterials with extended bonding. Uniaxial stress applied sequentially along different directions, with each step performing only partial saturation, could create higher-dimensional networks. Benzene can be thought of as the smallest possible section of a graphene network and reacts under uniaxial cold compression to form nanothreads. In contrast, the graphene layers in graphite form crystalline “transparent sp³ carbon” that reverts back to graphite unless quenched at low temperatures.^{26,27} The diversity of fully (degree 6) and partially (degree 4) saturated nanothread structures enumerated theoretically for benzene further suggests that multiple structures might be accessible from a single precursor molecule through appropriate control of pressure, stress, temperature, photochemistry, catalysts, and chemical initiators. These same parameters could also be exploited to reduce reaction pressure,^{10,28–30} as could precursors with reduced aromaticity. If the synthesis pressure could be reduced to ~6 GPa (at which >10⁶ kg/yr of diamond abrasive is manufactured),³¹ production could reach an industrial scale.

ASSOCIATED CONTENT

S Supporting Information

The Supporting Information is available free of charge on the ACS Publications website at DOI: 10.1021/jacs.7b09311.

Experiment methods and calculation details, Figure S1–15, and Table S1–2 (PDF)

Structures of benzene phase II (CIF)

Structures of polytwistane (CIF)

AUTHOR INFORMATION

Corresponding Author

*jbadding@chem.psu.edu

ORCID ®

Bo Chen: 0000-0002-5084-1321

Roald Hoffmann: 0000-0001-5369-6046

John V. Badding: 0000-0002-4517-830X

Present Address

□ Department of Civil and Environmental Engineering, and Department of Chemistry, George Washington University, Washington D.C., 20052, United States.

Notes

The authors declare no competing financial interest.

ACKNOWLEDGMENTS

This work was supported as part of the Energy Frontier Research in Extreme Environments (EFree) Center, an Energy Frontier Research Center funded by the U.S. Department of Energy, Office of Science under award number DE-SC0001057. Sample synthesis was performed at the Spallation Neutrons and Pressure (SNAP) beamline at the Spallation Neutron Source, a DOE Office of Science User Facility operated by the Oak Ridge National Laboratory. In situ X-ray diffraction experiments were performed at the High Pressure Collaborative Access Team (HPCAT) beamline 16 ID-B at the Advanced Photon Source (APS), Argonne National Laboratory (ANL). HPCAT operations are supported by DOE-NNSA under Award No. DE-NA0001974, with partial instrumentation funding by the National Science Foundation (NSF). We thank Jesse Smith, Ross Hrubiak, and Rich Ferry for their assistance during beamline data collection. In situ Raman data was collected at the High Pressure Synergetic Consortium (HPSyNc) facilities. We thank HPSyNc and Timothy Strobel (Carnegie Institution of Washington) for providing gas controllers. Hemant Yennawar assisted with in-house X-ray diffraction experiments at Penn State. Steven Juhl assisted with optical microscopy measurements at Penn State. Crystallographic pdb files of benzene phase II are available in the [Supporting Information](#).

REFERENCES

- (1) Dou, L. T.; Zheng, Y. H.; Shen, X. Q.; Wu, G.; Fields, K.; Hsu, W. C.; Zhou, H. P.; Yang, Y.; Wudl, F. *Science* **2014**, *343*, 272–277.
- (2) Lauher, J. W.; Fowler, F. W.; Goroff, N. S. *Acc. Chem. Res.* **2008**, *41*, 1215–1229.
- (3) Yamanaka, S.; Kini, N. S.; Kubo, A.; Jida, S.; Kuramoto, H. *J. Am. Chem. Soc.* **2008**, *130*, 4303–4309.
- (4) Thess, A.; Lee, R.; Nikolaev, P.; Dai, H. J.; Petit, P.; Robert, J.; Xu, C. H.; Lee, Y. H.; Kim, S. G.; Rinzler, A. G.; Colbert, D. T.; Scuseria, G. E.; Tomanek, D.; Fischer, J. E.; Smalley, R. E. *Science* **1996**, *273*, 483–487.
- (5) Bini, R.; Schettino, V. *Materials under extreme conditions: molecular crystals at high pressure*; Imperial College Press: London, 2014.
- (6) Ciabini, L.; Santoro, M.; Gorelli, F. A.; Bini, R.; Schettino, V.; Raugei, S. *Nat. Mater.* **2007**, *6*, 39–43.
- (7) McBride, J. M.; Segmuller, B. E.; Hollingsworth, M. D.; Mills, D. E.; Weber, B. A. *Science* **1986**, *234*, 830–835.
- (8) Piermarini, G. J.; Mighell, A. D.; Weir, C. E.; Block, S. *Science* **1969**, *165*, 1250–1255.
- (9) Diercks, C. S.; Yaghi, O. M. *Science* **2017**, *355*, 923–931.
- (10) Fitzgibbons, T. C.; Guthrie, M.; Xu, E. S.; Crespi, V. H.; Davidowski, S. K.; Cody, G. D.; Alem, N.; Badding, J. V. *Nat. Mater.* **2015**, *14*, 43–47.
- (11) Maryasin, B.; Olbrich, M.; Trauner, D.; Ochsenfeld, C. *J. Chem. Theory Comput.* **2015**, *11*, 1020–1026.
- (12) Olbrich, M.; Mayer, P.; Trauner, D. *J. Org. Chem.* **2015**, *80*, 2042–2055.
- (13) Chen, B.; Hoffmann, R.; Ashcroft, N. W.; Badding, J.; Xu, E. S.; Crespi, V. *J. Am. Chem. Soc.* **2015**, *137*, 14373–14386.
- (14) Xu, E. S.; Lammert, P. E.; Crespi, V. H. *Nano Lett.* **2015**, *15*, 5124–5130.
- (15) Roman, R. E.; Kwan, K.; Cranford, S. W. *Nano Lett.* **2015**, *15*, 1585–1590.
- (16) Zhan, H.; Zhang, G.; Tan, V. B. C.; Cheng, Y.; Bell, J. M.; Zhang, Y.-W.; Gu, Y. *Nanoscale* **2016**, *8*, 11177–11184.
- (17) Halasz, I. *Cryst. Growth Des.* **2010**, *10*, 2817–2823.
- (18) Stojkovic, D.; Zhang, P. H.; Crespi, V. H. *Phys. Rev. Lett.* **2001**, *87*, 125502.
- (19) Wang, Z. W.; Schliehe, C.; Wang, T.; Nagaoka, Y.; Cao, Y. C.; Bassett, W. A.; Wu, H. M.; Fan, H. Y.; Weller, H. *J. Am. Chem. Soc.* **2011**, *133*, 14484–14487.
- (20) Boldyreva, E.; Dera, P. *High-Pressure Crystallography From Fundamental Phenomena to Technological Applications*; Springer: Dordrecht, The Netherlands, 2010.
- (21) Hahn, T. *International Tables for Crystallography Vol. A: Space Group Symmetry*, 5th ed.; Springer: Dordrecht, The Netherlands, 2005.
- (22) Scheffer, J. R.; Scott, C. *Science* **2001**, *291*, 1712–1713.
- (23) Plimpton, S. *J. Comput. Phys.* **1995**, *117*, 1–19.
- (24) Breitling, S. M.; Jones, A. D.; Boyd, R. H. *J. Chem. Phys.* **1971**, *54*, 3959–3964.
- (25) Lee, W. Y.; Slutsky, L. *J. J. Phys. Chem.* **1975**, *79*, 2602–2604.
- (26) Miller, E. D.; Nesting, D. C.; Badding, J. V. *Chem. Mater.* **1997**, *9*, 18–22.
- (27) Utsumi, W.; Yagi, T. *Science* **1991**, *252*, 1542–1544.
- (28) Bini, R. *Acc. Chem. Res.* **2004**, *37*, 95–101.
- (29) Ciabini, L.; Santoro, M.; Bini, R.; Schettino, V. *Phys. Rev. Lett.* **2002**, *88*, 085505.
- (30) Ciabini, L.; Gorelli, F. A.; Santoro, M.; Bini, R.; Schettino, V.; Mezouar, M. *Phys. Rev. B: Condens. Matter Mater. Phys.* **2005**, *72*, 094108.
- (31) United States Geological Survey Diamond Report. <https://minerals.usgs.gov/minerals/pubs/commodity/diamond/mcs-2016-diamo.pdf>.